Preprints of the 21st IFAC World Congress (Virtual)
Berlin, Germany, July 12-17, 2020

Active Damping of Parallel Robots Driven by Elastic Cables using On-Off Actuators through Model Predictive Control Allocation

Imane Khayour, Sylvain Durand, Loïc Cuvillon, Jacques Gangloff

ICube Laboratory, Strasbourg University, INSA Strasbourg, France
(e-mail: {khayour, l.cuvillon, jacques.gangloff}@unistra.fr,
sylvain.durand@insa-strasbourg.fr).

Abstract: This work studies the vibration rejection on elastic cable-driven parallel robots (CDPRs). Additional cold-gas thrusters are embedded on the robot in order to improve the rejection bandwidth. Such Unilateral Force Generators (UFGs) work as on-off actuators. Under the framework of optimal control, a Model Predictive Control (MPC) is designed to compute the control law and allocate the control signals to the available actuators by assigning their binary on-off states, thus forming a Mixed Integer Quadratic Programming (MIQP)-based MPC controller. Simulations highlight the benefits of the proposed predictive approach that yields a better rejection, fuel efficiency, and a reduced switching between ON and OFF states with respect to previous approaches.

Keywords: Predictive control, on-off actuator, robotic manipulator.

1. INTRODUCTION

The rigid links of traditional parallel robots were replaced by flexible cables for the first time in the 1980s, according to Qian et al. (2018). The goal was to increase the speed and acceleration of the manipulator thanks to lower cable inertia, and reach wider workspaces thanks to a better scalability. The drawback is an increased flexibility that yields vibrations degrading performance and accuracy of such a robotic architecture.

Usual actuators for Cable-Driven Parallel Robots (CDPRs) are winches. They can be mounted on the supporting structure or on the platform and are used to control the pose of the platform. They can also be used to reject vibrations, but they generally act with relatively slow dynamics. To better handle these vibrations, recent works proposed to embed additional actuators on the platform. Thus, the cable winches are used for the pose regulation and trajectory tracking, while extra actuators focus on active damping of the oscillations. For instance, Weber et al. (2014) assessed reaction wheels (commonly used in satellite stabilization) on a planar CDPR. Lesellier et al. (2018) used rotating arms to actively stabilize a 3-DoF planar CDPR. Rotating arms were also combined with cable winches in Qi et al. (2019) for both vibration control and trajectory tracking of a hybrid cable-driven robot. Binary or on-off actuators, such as cold-gas thrusters, have also been evaluated in Sellet et al. (2019). Such a technology can only take ON or OFF values and the actuator, an electromagnetic valve, has only two states: open or closed. These actuators may be difficult to implement (because of the need for an embedded pressure buffer and a trailing pipe that supplies the compressed air) and to control, due to their switched behavior. Nonetheless, they have a faster response time than reaction wheels or rotating arms. Furthermore, thrusters do not alter the platform inertia and can maintain a unilateral force over an extended period of time compared to inertia-based actuators that are prone to saturation.

Dedicated actuators with fast dynamics is a promising solution to improve active damping, but the controlled system generally becomes over-actuated. Several approaches studying control allocation of over-actuated systems can be found in literature. In particular, a Model Predictive Control (MPC) can be employed to both design the control law and allocate the various embedded actuators under the framework of optimal control. The so-called Model Predictive Control Allocation (MPCA) methods were reviewed by Johansen and Fossen (2013). They received a lot of interest in many fields like marine vessels, underwater systems and mobile vehicles. For example, in order to maintain an over-actuated marine vessel to a certain position, known as dynamic positioning, Veksler et al. (2016) implemented an algorithm combining both the position control and the thruster allocation into one predictive controller. Bächle et al. (2015) studied the performance of a MPCA on an over-actuated vehicle drive-train equipped with motors and brakes and designed an algorithm suitable for real-time implementation. Qian et al. (2016) resolved the trajectory planning of an autonomous vehicle under the predictive control framework. Moreover, as their actuators have both continuous and discrete output values, the optimization problem was formulated as a Mixed Integer Quadratic Programming (MIQP).

In the present paper, a model predictive control allocation for an elastic CDPR with embedded Unilateral Force

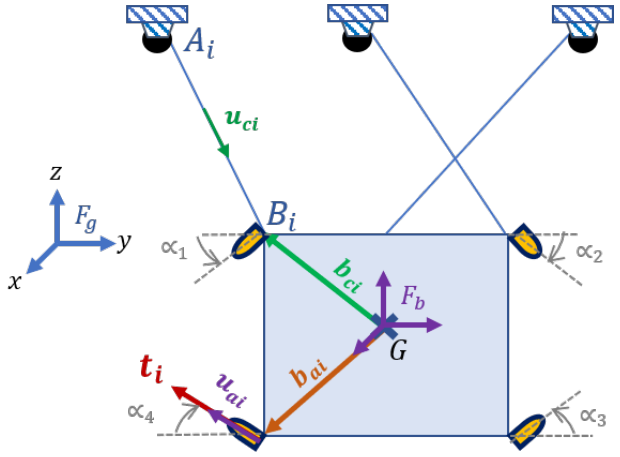

Fig. 1. CDPR planar configuration.

Generators (UFGs) is proposed. The actuator constraints are explicitly considered, particularly the on-off behavior of the cold-gas thrusters. Note that this work focuses on oscillation rejection using fast UFGs. The control of the winches is not considered here. The remainder of the paper is organized as follows. Section 2 describes the over-actuated elastic CDPR and the embedded on-off actuators along with their dynamic equations. In Section 3, a two-stage controller (speed control and control allocation) is briefly introduced, derived from Sellet et al. (2019). The MIQP-based MPCA is also detailed, especially when binary actuators are used. The predictive controller is then studied for the case of a 3-DoF (Degree of Freedom) planar robot in section 4. Simulation results are used to assess the proposal. A conclusion is finally given in Section 5.

2. SYSTEM DESCRIPTION

The system of this study is a n-DoF cable-driven parallel robot whose platform is moved using n_c elastic cables. Additional unidirectional forces can be generated by n_a actuators mounted on the platform (see Fig. 1). Let $\mathbf{x} = [\mathbf{p}^T \boldsymbol{\theta}^T]^T \in \mathbb{R}^n$ be the pose of the CDPR platform in the inertial frame $\mathcal{F}_g$, with $\mathbf{p}$ the vector of coordinates of its center of gravity G and $\boldsymbol{\theta}$ the vector of Euler angles describing its orientation.

2.1 UFG Actuators

The unidirectional force generators (UFGs), like cold-gas thrusters, are mounted on the platform. Their thrust direction $\mathbf{u_{ai}}$ is constant into the platform frame $\mathcal{F}_b$, as represented in Fig. 1, and the thrust delivered is positive of magnitude $t_i \geq 0$.

Let $\mathbf{t} = [t_1, \ldots, t_{n_a}]^T$ be the vector of the thrusts for all UFGs. The resulting wrench on the platform is given by:

$$\begin{bmatrix} {}^b\mathbf{F_a} \\ {}^b\mathbf{N_a} \end{bmatrix} = \underbrace{-\begin{bmatrix} {}^b\mathbf{u_{a1}} & \cdots & {}^b\mathbf{u_{a n_a}} \\ {}^b\mathbf{b_{a1}} \times {}^b\mathbf{u_{a1}} & \cdots & {}^b\mathbf{b_{a n_a}} \times {}^b\mathbf{u_{a n_a}} \end{bmatrix}}_{\mathbf{A_a}} \mathbf{t} \tag{1}$$

where $\mathbf{b_{ai}}$ is the vector of coordinates between the gravity center G and the thruster position on the platform, $\mathbf{F_a}$ and $\mathbf{N_a}$ are the forces and moments respectively applied by the different UFGs, $\mathbf{A_a}$ is the constant configuration matrix of the embedded actuators. The wrench matrix $\mathbf{W_a} \in \mathbb{R}^{n \times n_a}$ expressed in the inertial frame $\mathcal{F}_g$ is:

$$\begin{bmatrix} {}^g\mathbf{F_a} \\ {}^g\mathbf{N_a} \end{bmatrix} = \underbrace{\begin{bmatrix} \mathbf{R_{gb}}(\mathbf{x}) & \mathbf{0} \\ \mathbf{0} & \mathbf{R_{gb}}(\mathbf{x}) \end{bmatrix} \mathbf{A_a}}_{\mathbf{W_a}(\mathbf{x})} \mathbf{t} \tag{2}$$

where $\mathbf{R_{gb}}$ is the rotation matrix between $\mathcal{F}_g$ and $\mathcal{F}_b$.

Finally, the UFGs are considered as binary actuators with:

$$t_i = T_{\max} u_i \tag{3}$$

where $u_i \in \{0, 1\}$ and $T_{\max}$ is the thrust when the actuator is on. In the present case of cold-gas thrusters, high-speed electromagnetic valves (like the Festo TMMHJ-9-QS-6-HF) are controlling the airflow by only switching their input between on and off.

The wrench matrix $\mathbf{W_a} \in \mathbb{R}^{n \times n_a}$, as a function of the vector $\mathbf{u} = [u_1, \ldots, u_{n_a}]$ of the binary inputs, becomes:

$$\begin{bmatrix} {}^g\mathbf{F_a} \\ {}^g\mathbf{N_a} \end{bmatrix} = T_{\max} \mathbf{W_a}(\mathbf{x})\, \mathbf{u} \tag{4}$$

2.2 CDPR dynamics

Using Newton-Euler formulation, the dynamic equations of the CDPR driven by thrusters, elastic cables and submitted to gravity $\mathbf{g}$ expressed in $\mathcal{F}_g$ are given by:

$$\begin{bmatrix} m\mathbb{I} & \mathbf{0} \\ \mathbf{0} & \mathbf{I_g} \end{bmatrix} \begin{bmatrix} \ddot{\mathbf{p}} \\ \dot{\boldsymbol{\omega}} \end{bmatrix} + \begin{bmatrix} \mathbf{0} \\ \boldsymbol{\omega} \times \mathbf{I_g}\boldsymbol{\omega} \end{bmatrix} + \begin{bmatrix} -m\mathbf{g} \\ \mathbf{0} \end{bmatrix} = \begin{bmatrix} {}^g\mathbf{F} \\ {}^g\mathbf{N} \end{bmatrix} \tag{5}$$

with $\mathbf{p}$ the coordinates of G and $\boldsymbol{\omega}$ the angular velocity of the platform. The platform is characterized by its mass m and its inertia matrix $\mathbf{I_g}(\mathbf{x})$ expressed in the inertial frame. $\mathbf{F_c}$ and $\mathbf{N_c}$ are the forces and moments respectively exerted on the platform by the cables.

The wrench matrix $\mathbf{W_c} \in \mathbb{R}^{n \times n_c}$ maps the cable tensions $\boldsymbol{\tau}$ to the force $\mathbf{F_c}$ and moment $\mathbf{N_c}$ applied to the platform:

$$\begin{bmatrix} {}^g\mathbf{F_c} \\ {}^g\mathbf{N_c} \end{bmatrix} = \mathbf{W_c}(\mathbf{x})\boldsymbol{\tau} \tag{6}$$

with

$$\mathbf{W_c} = -\begin{bmatrix} {}^g\mathbf{u_{c1}} & \cdots & {}^g\mathbf{u_{c n_c}} \\ {}^g\mathbf{b_{c1}} \times {}^g\mathbf{u_{c1}} & \cdots & {}^g\mathbf{b_{c n_c}} \times {}^g\mathbf{u_{c n_c}} \end{bmatrix}$$

where ${}^g\mathbf{u_{ci}}$ is the coordinates in $\mathcal{F}_g$ of the i^{th} cable unit direction vector and ${}^g\mathbf{b_{c_i}}$ the coordinates of the vector between G and the cable attachment point B_i (see Fig. 1).

The cables and embedded actuators apply on the platform a total force $\mathbf{F}$ and moment $\mathbf{N}$:

$$\begin{bmatrix} {}^g\mathbf{F} \\ {}^g\mathbf{N} \end{bmatrix} = \begin{bmatrix} {}^g\mathbf{F_c} \\ {}^g\mathbf{N_c} \end{bmatrix} + \begin{bmatrix} {}^g\mathbf{F_a} \\ {}^g\mathbf{N_a} \end{bmatrix} = [\mathbf{W_c} \quad T_{\max}\mathbf{W_a}] \begin{bmatrix} \boldsymbol{\tau} \\ \mathbf{u} \end{bmatrix} \tag{7}$$

where $\boldsymbol{\tau}$ is the cable tensions and $\mathbf{u}$ the UFGs binary inputs. Let $\mathbf{S}(\boldsymbol{\theta})$ be the matrix that links the time derivative of the angular coordinates $\boldsymbol{\theta}$ to the angular velocity $\boldsymbol{\omega}$.

$$\boldsymbol{\omega} = \mathbf{S}(\boldsymbol{\theta})\dot{\boldsymbol{\theta}} \tag{8}$$

Thereby, the dynamic equation of the CDPR can be expressed as (Begey et al. (2018)):

$$\mathbf{M}(\mathbf{x})\ddot{\mathbf{x}} + \mathbf{C}(\mathbf{x}, \dot{\mathbf{x}})\dot{\mathbf{x}} + \mathbf{G}(\mathbf{x}) = \mathbf{W}(\mathbf{x}) \begin{bmatrix} \boldsymbol{\tau} \\ \mathbf{u} \end{bmatrix} \tag{9}$$

- the mass matrix or kinetic energy matrix:

$$\mathbf{M}(\mathbf{x}) = \begin{bmatrix} m\mathbb{I} & \mathbf{0} \\ \mathbf{0} & \mathbf{S}^T\mathbf{I_f}\mathbf{S} \end{bmatrix} \tag{10}$$

- the matrix of centrifugal and Coriolis forces:

$$\mathbf{C}(\mathbf{x}, \dot{\mathbf{x}}) = \begin{bmatrix} \mathbf{0} \\ \mathbf{S}^T(\mathbf{I_f}\dot{\mathbf{S}}\dot{\boldsymbol{\theta}} + \mathbf{S}\,\dot{\boldsymbol{\theta}} \times \mathbf{I_f}\mathbf{S}\,\dot{\boldsymbol{\theta}}) \end{bmatrix} \tag{11}$$

- the wrench matrix $\mathbf{W} \in \mathbb{R}^{n\times(n_a+n_c)}$:

$$\mathbf{W}(\mathbf{x}) = [\mathbf{W_{cx}}\ \ \mathbf{W_{ax}}]\,(\mathbf{x}) \tag{12}$$

with $\mathbf{W_{cx}} = \begin{bmatrix} \mathbb{I} & \mathbf{0} \\ \mathbf{0} & \mathbf{S}^T \end{bmatrix} \mathbf{W_c}$, $\mathbf{W_{ax}} = T_{\max} \begin{bmatrix} \mathbb{I} & \mathbf{0} \\ \mathbf{0} & \mathbf{S}^T \end{bmatrix} \mathbf{W_a}$

- the gravity matrix: $\mathbf{G} = \begin{bmatrix} -m\mathbf{g} \\ \mathbf{0} \end{bmatrix}$

The cable under tension is considered as a straight line between its attachment points, as depicted in Fig. 1. The cable length vector is $\mathbf{l_1}(\mathbf{x})$, the distance between the attachment points. Let $\mathbf{l_2} = [l_{21}, \ldots, l_{2n_c}]^T$ be the vector of cable free lengths when the cable tension is zero. The vector of the cable elongations is $[\mathbf{l_1}(\mathbf{x}) - \mathbf{l_2}]$. The cable tension is thus described by the relation:

$$\boldsymbol{\tau} = \mathbf{K_c}(\mathbf{l_2})[\mathbf{l_1}(\mathbf{x}) - \mathbf{l_2}] + \mathbf{F_c}[\dot{\mathbf{l}}_1 - \dot{\mathbf{l}}_2] \tag{13}$$

where $\mathbf{F_c} = \mathrm{diag}(f_c, \ldots, f_c)$, with f_c the cable friction coefficient, and $\mathbf{K_c} = \mathrm{diag}(\frac{k_s}{l_{21}}, \ldots, \frac{k_s}{l_{2n_c}})$, with k_s the cable specific stiffness, are diagonal matrices.

Using the winch actuators to roll and unroll the cables, the free cable length $\mathbf{l}_2$ and therefore the cable tension can be modified. However, as the paper is focused on active damping of oscillations using UFG embedded actuators, winch actuation is not considered for the remainder of the paper. Thus $\mathbf{l}_2$ is considered as a constant vector.

3. CONTROL DESIGN

As a wrench disturbance is exerted on the robot platform, it oscillates around its equilibrium state. The objective of the controller is to bring back the CDPR position to its resting position by allocating the UFG thrusts. This section presents two approaches of disturbance rejection for the CDPR (9), that will be compared in the sequel.

3.1 Two-stage control strategy

The first method is a two-stage control design (speed control and control allocation), as previously proposed in Sellet et al. (2019) and illustrated in Fig. 2. For the first stage, a velocity feedback is introduced to damp the oscillations. This strategy emulates a friction wrench in opposition to the velocity of the platform oscillations. The second stage is a thrust allocation method. It assigns the forces of the embedded thrusters, taking into account their saturation, in order to generate the desired friction wrench and to ensure positivity of the thrusts.

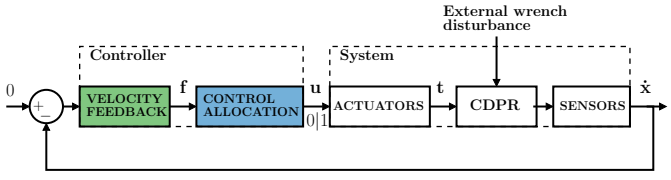

Fig. 2. Two-stage control strategy with velocity feedback and control allocation.

Control design: The friction wrench created by the on-board UFGs is in the opposite direction of the oscillation velocity $\dot{\mathbf{x}}$ thanks to a velocity feedback:

$$\mathbf{f} = -\mathbf{K_f}\,\dot{\mathbf{x}} \tag{14}$$

where $\mathbf{K_f} = \mathrm{diag}(k_1, \ldots, k_n)$ is a positive definite and constant diagonal matrix of tunable gains. They allow for fine-tuning of the damping force along the main vibration modes.

Thrust allocation: The desired wrench $\mathbf{f} \in \mathbb{R}^n$ is mapped to the thrust vector $\mathbf{t} \in \mathbb{R}^{n_a}$ of the cold-gas thruster by the wrench matrix $\mathbf{W_{ax}} \in \mathbb{R}^{n\times n_a}$ defined in (12):

$$\mathbf{W_{ax}}\mathbf{t} = \mathbf{f} \tag{15}$$

If $\mathbf{W_a}$ is full rank, the problem is under-determined and has an infinity number of solutions of the form :

$$\mathbf{t} = (\mathbf{W_{ax}})^{+}\mathbf{f} + \mathcal{N}\boldsymbol{\lambda} \tag{16}$$

where $()^+$ is the Moore-Penrose pseudo-inverse and $\mathcal{N} \in \mathbb{R}^{na\times r}$ is a basis of $\ker\{\mathbf{W_{ax}}\}$ with $r = n_a - n$, the degree of redundancy of the actuation. The vector $\boldsymbol{\lambda} \in \mathbb{R}^r$ can be freely chosen to select a particular solution, such that the actuator constraints $0 \le t_i \le T_{\max}$ are verified.

Let illustrate the thrust allocation on a planar 3-DOF CDPR with a symmetrical configuration of four thrusters as in Fig. 1. The degree of redundancy is $r = 1$ and $\mathcal{N} = \mathbf{I}_{4\times1} = [1\ 1\ 1\ 1]^T$ is a basis of the wrench matrix null space. It means that when all the thrusters are generating the same force, the resulting wrench on the platform is null due to the symmetrical configuration. To ensure the positivity of the thrust ($t_i \ge 0$), λ is chosen as:

$$\lambda = -\min_i \left((\mathbf{W_{ax}})^{+}\mathbf{f}\right)_i \tag{17}$$

such that

$$\mathbf{t} = (\mathbf{W_a}\mathbf{x})^{+}\mathbf{f} - \min_i \left((\mathbf{W_{ax}})^{+}\mathbf{f}\right)_i \mathbf{I}_{4\times1} \tag{18}$$

However, if $\exists i$, such that $t_i > T_{\max}$ in the solution of (18), the desired wrench $\mathbf{f}$ is out of reach for the thrusters. The vector $\mathbf{t}$, and therefore wrench $\mathbf{f}$, is then scaled down by a factor β to meet the saturation limit of all the thrusters:

$$\mathbf{t}' = \beta\,\mathbf{t} \ \text{ with } \ \beta = \mathrm{sat}\left(\frac{T_{\max}}{\max_i(t_i)}\right) \tag{19}$$

Finally, the continuous thrust $\mathbf{t}$ is converted in a binary on-off control signal $\mathbf{u}$ for the thruster valves. A PWM modulation of a high frequency carrier is one classic solution to generate an equivalent average thrust with a binary signal:

$$\mathbf{u} = \mathrm{PWM}(\mathbf{t}) \tag{20}$$

Another one is to send the thrust signal $\mathbf{t}$ in a Schmitt trigger as detailed later in section 4.

The stability of this two-stage control has been proved in Sellet et al. (2019) based on Lyapunov stability theory.

3.2 Predictive control strategy

The second approach consists of a single stage which directly allocates the thrusters to damp the disturbances. It combines both the *control design* and *thrust allocation* of the previous approach in a predictive framework (see Fig. 3). One of the main features of MPC is handling actuator constraints explicitly in the optimization problem. Therefore, the limitations of the UFGs can be expressed

as binary constraints. These discrete or binary constraints are handled through a so-called Mixed-Integer (MI) MPC.

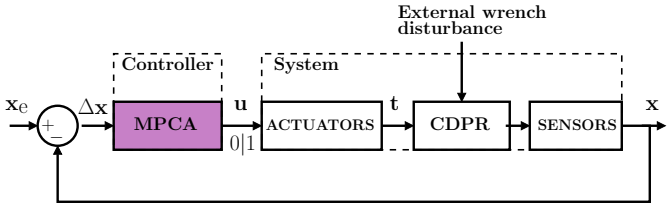

Fig. 3. MIQP-based MPCA strategy.

Linear plant: In order to compute the MPC controller, the CDPR dynamics are first linearized around an equilibrium point $[\mathbf{x}^T, \dot{\mathbf{x}}^T, \boldsymbol{\tau}, \mathbf{u}]^T = [\mathbf{x_e}^T, \mathbf{0}^T, \boldsymbol{\tau}_e, \mathbf{0}^T]^T$. The resulting linear model is equivalent to a n-DOF mass-spring system, that is convenient for analysing and modeling the vibration modes. Let the pose of the platform relative to its static position around the equilibrium point $\mathbf{x_e}$ be defined by the deviation $\Delta\mathbf{x}$ such as:

$$\Delta\mathbf{x} = \mathbf{x} - \mathbf{x_e} \tag{21}$$

Then, the system (9) becomes:

$$\mathbf{M}(\mathbf{x_e})\,\Delta\ddot{\mathbf{x}} + \mathbf{K_x}(\mathbf{x_e}, \boldsymbol{\tau}_e)\,\Delta\mathbf{x} = \mathbf{W_{ax}}(\mathbf{x_e})\mathbf{u} \tag{22}$$

where $\mathbf{W_{ax}}$ is the wrench matrix of the on-off thrusters, $\mathbf{M}$ is the mass matrix of the platform and the cable friction is neglected. The stiffness matrix of the platform is $\mathbf{K_x}$, which is a function of the cable stiffness matrix $\mathbf{K_c}$ and the antagonist cable tensions $\boldsymbol{\tau}_e$. The stiffness matrix is computed through differentiating the cable wrench with respect to the pose $\mathbf{x}$ of the end effector. The derivation of the stiffness matrix for CDPR and its expression can be found in Behzadipour and Khajepour (2006).

Let the state vector for the linearized system be:

$$\underline{\mathbf{x}} = [\Delta\mathbf{x}^T, \Delta\dot{\mathbf{x}}^T]^T \tag{23}$$

Then, a linearized state-space representation is:

$$\begin{cases} \dot{\underline{\mathbf{x}}} = A\underline{\mathbf{x}} + B\mathbf{u} \\ \mathbf{y} = \Delta\mathbf{x} = C\underline{\mathbf{x}} \end{cases} \tag{24}$$

with $A = \begin{bmatrix} \mathbf{0} & \mathbb{I} \\ -\mathbf{M^{-1}K_x} & \mathbf{0} \end{bmatrix}$, $B = \begin{bmatrix} \mathbf{0} \\ \mathbf{M^{-1}W_{ax}} \end{bmatrix}$ and $C = \begin{bmatrix} \mathbb{I} \\ \mathbf{0} \end{bmatrix}$.

Finally, a discrete-time model can be calculated assuming zero-order hold:

$$\begin{cases} \underline{\mathbf{x}}_{k+1} &= A_d\underline{\mathbf{x}}_k + B_d\mathbf{u}_k \\ \mathbf{y}_k &= \Delta\mathbf{x}_k = C\underline{\mathbf{x}}_k \end{cases} \tag{25}$$

MIQP-based MPC: The predictive controller runs an optimization over a number of time samples N called prediction horizon (Maciejowski (2002)). Based on the prediction model (25), the predictive controller computes a nearly optimal control sequence $\mathbf{U} = [\mathbf{u}_0, \ldots, \mathbf{u}_{N-1}]$ with respect to the actuator constraints:

$$\forall i, u_{ki} \in \{0, 1\} \text{ in } \mathbf{u}_k = [u_{k1}, \ldots u_{kn_a}]^T \tag{26}$$

The first control signal sample $\mathbf{u_0}$ of the sequence $\mathbf{U}$ is applied to the system and the optimization problem is solved again at the next sample time. The goal of the optimization problem is to find the sequence $\mathbf{U}$ that minimizes the quadratic cost function J defined as :

$$J = \min_{\mathbf{U}} \sum_{k=0}^{N-1} \underbrace{\|\mathbf{y}_k - \mathbf{y}_{ref}\|^2_{\mathbf{Q}}}_{V_{\Delta x}} + \underbrace{\|\mathbf{u}_k\|^2_{\mathbf{R}}}_{V_u} + \underbrace{\|\underline{\mathbf{x}}_N\|^2_{\mathbf{P}}}_{V_f} \tag{27}$$

Table 1. Parameters and constraints.

Parameter	Symbol	Value	Unit
Platform mass	m_p	3.195	kg
Platform inertia	I_p	0.066	kgm^2
Cable specific stiffness	k_s	504	N
Damping coefficient	f_c	7	$\mathrm{N\,m^{-1}\,s}$
Maximum thrust limit	T_{max}	2	N

where $\|v\|^2_{\mathbf{X}} = v^T\mathbf{X}v$, $\mathbf{R} > 0$ and $\mathbf{Q} \geq 0$ are weight matrices that penalize respectively the control energy (V_u) and the quadratic error with respect to its reference pose ($V_{\Delta x}$). The term V_f in the cost function (27) is a terminal cost introduced to ensure the closed-loop stability with an appropriate choice of the weight matrix $P \geq 0$ (Bemporad and Morari (1999), Allan et al. (2016)).

The predictive control problem to solve at each sampling time is defined by:

i) the cost function (27);
ii) the system model (25) with its initial state $\underline{\mathbf{x}}_\mathbf{0}$;
iii) the input constraints (26).

This problem is equivalent to a Mixed-Integer Quadratic Programming (MIQP) problem, as stated by Bemporad and Naik (2018).

4. SIMULATION RESULTS: APPLICATION TO A 3-DOF PLANAR ELASTIC CDPR

To validate the control strategy and without loss of generality, a planar CDPR suspended by 3 cables with embedded air thrusters is studied here. Although only simulations are presented in this paper, the experimental validation of the model and the two-stage control strategy have been carried out by Sellet et al. (2019) on this same CDPR.

The nonlinear model (9) of this CDPR is simulated with Simulink's Simscape Multibody™ toolbox to reproduce the behaviour of the real system. Parameters and thruster constraints are defined in Table 1. The pose of the platform in the world frame $\mathcal{F}_g$ is described by the vector $\mathbf{x} = [y\ z\ \theta]^T \in \mathbb{R}^3$. Around a static equilibrium pose $\mathbf{x_e} = [y_e\ z_e\ \theta_e]^T$, the system behavior is similar to a 3-DoF coupled oscillator with low frequency and low-damped modes. This results from the low stiffness and small inner friction of the long cables used here made of polyamide (Capperlan™ Line clear 0.55 mm).

In this section, both control strategies (introduced in Section 3) are implemented on MATLAB/Simulink and the performance of vibration rejection is compared.

4.1 Two-stage control strategy

The platform velocity $\dot{\mathbf{x}}$ is used to compute a friction wrench in order to dissipate all the vibration energy. The best damping is achieved when $\mathbf{K_F}$ is tuned close to $\mathbb{I}_{3\times3}$. The wrench is sent to the control allocation block to generate the equivalent on-off thrusts to be applied by the actuators (see Fig. 2). Two versions of the input signal modulation are implemented, derived from Sellet et al. (2019):

(1) *Pulse Width Modulation (PWM):* The 100 Hz carrier frequency of the PWM is selected in accordance with

the opening and closing time of the high-speed valve (2 ms). To avoid chattering of the control signal, a dead zone is added to the wrench. Thus, if $\mathbf{f} \leq [0.05\,\text{N}, 0.05\,\text{N}, 0.05\,\text{N m}]^T$, the control signal of the thrusters is $t_i = 0$.

(2) *Schmitt Trigger (ST):* The binary signal sent to the thrusters is modulated by using a Schmitt trigger after the control allocation block with the same dead zone on the wrench than PWM. The upper and lower thresholds are fixed respectively to 0.3 N and 0.1 N. When $t_i > 0.3\,\text{N}$, the output of the Schmitt Trigger is 1, and so the valve is open. When $t_i < 0.1\,\text{N}$, the output is zero and the valve is closed.

4.2 MIQP-based MPCA strategy

For the MPC approach, the model is linearized around its equilibrium position $\mathbf{x_0}$, as in (24):

$$\begin{cases} \dot{\underline{\mathbf{x}}} = A\underline{\mathbf{x}} + B\mathbf{u} \\ \mathbf{y} = \Delta\mathbf{x} = C\underline{\mathbf{x}} \end{cases} \tag{28}$$

where $\underline{\mathbf{x}} = [\Delta\mathbf{x}^T, \Delta\dot{\mathbf{x}}^T]^T = [\Delta y, \Delta z, \Delta\theta, \Delta\dot{y}, \Delta\dot{z}, \Delta\dot{\theta}]^T$. Matrices A and B depend on the inertia matrix of the platform $\mathbf{M}$ and the stiffness matrix $\mathbf{K_x}$:

$$\mathbf{M} = \text{diag}(m_p, m_p, I_p) \qquad \mathbf{K_x} = \text{diag}(k_1, k_2, k_3) \tag{29}$$

where m_p and I_p are mass and inertia of the platform respectively, k_i is i^{th} cable stiffness, and $\mathbf{W_c}$ is the cable wrench matrix defined in section 2.

Note that in the planar case, $\mathbf{S} = 1$ in (8). The wrench matrix $\mathbf{W_{ax}}$ is given by:

$$\begin{bmatrix} F_y \\ F_z \\ N_x \end{bmatrix} = \mathbf{W_{ax}}(\mathbf{x_e}) \begin{bmatrix} u_1 \\ u_2 \\ u_3 \\ u_4 \end{bmatrix}, \text{ with} \tag{30}$$

$$\mathbf{W_{ax}} = T_{\max} \begin{bmatrix} \cdots & \cos(\alpha_i + \theta_0) & \cdots \\ \cdots & \sin(\alpha_i + \theta_0) & \cdots \\ \cdots & b_{ay_i}\sin(\alpha_i + \theta_0) - b_{az_i}\cos(\alpha_i + \theta_0) & \cdots \end{bmatrix} \tag{31}$$

where α_i is the orientation of the i^{th} thruster and $[0, b_{ay_i}, b_{az_i}]^T$, the vector of its attachment point coordinates b_{a_i} in the body frame.

Then, the system (28) is discretized assuming zero-order hold at a sampling period T_s yielding the prediction model (25). Based on this discrete-time linear model, a predictive controller is synthesized in order to damp the oscillations. Here, the reference is zero, i.e. a null deviation from the equilibrium pose. This yields $\mathbf{y}_{ref} = \Delta\mathbf{x}_{ref} = \mathbf{0}$ and the quadratic cost (27) becomes:

$$J = \min_{\mathbf{U}} \sum_{k=0}^{N-1} \left\| \begin{matrix} \Delta y_k \\ \Delta z_k \\ \Delta\theta_k \end{matrix} \right\|_{\mathbf{Q}}^2 + \|\mathbf{u}_k\|_{\mathbf{R}}^2 + \|\underline{\mathbf{x}}_N\|_{\mathbf{P}}^2 \tag{32}$$

with the weighting matrices:

$$\mathbf{Q} = \text{diag}(q_y, q_z, q_\theta),\ \mathbf{R} = r\mathbb{I}_4,\ \text{and}\ \mathbf{P} = \text{diag}(\mathbf{Q}, \mathbf{0}) \tag{33}$$

where q_y, q_z, q_θ and r are the tuning parameters of the MPC controller.

The controller is implemented using Yalmip created by Löfberg (2004) and using the Gurobi solver based on a branch-and-bound algorithm. Extensive simulations were performed to tune the parameters in order to achieve the best performance. The resulting parameters are listed in Table 2.

Table 2. MPC parameters.

Parameter	Value	Parameter	Value
r	0.1	T_s	0.01 s
$\{q_y, q_z, q_\theta\}$	$\{10, 40, 10\}$	N	40

4.3 Evaluation and comparison of the controllers

Performance of the MIQP-based MPCA is compared to the two-stage controller with both PWM and ST modulation. Simulations are carried out by disturbing the initial pose of the nonlinear simulation model of the CDPR, away from its equilibrium position.

The performance criteria are: $\int |u_i|$ the air consumed during the rejection, N_s the number of switchings of the UFGs, the damping time T_d and the improvement ratio of the rejection. The damping time T_d is defined as the time required for the vibration amplitude to reach and settle within the ± 1 mm or ± 5 mrad range. The improvement ratios are computed with RMS (in %) with respect to the open-loop response for each component x of the deviation vector Δx. The results are summed up in Table 3.

Table 3. Comparison of the different methods.

	N_s	T_d [s]			$\int \lvert u_i \rvert$	Improvement		
		y	z	θ		y	z	θ
PWM	386	3.944	1.844	2.418	2360	36%	58%	25%
ST	364	4.069	1.577	2.534	2664	35%	54%	26%
MPC	**40**	**1.104**	**1.081**	**0.797**	**348**	**40%**	**60%**	**38%**

The predictive controller (MPC) has the fastest damping time in the three directions, as highlighted in Fig. 4. Furthermore, the MPC dampens the system while consuming 7 times less gas than the other strategies (comparing $\int |u_i|$ results in Table 3). This criterion is very important when the air tank is embedded on the robot end-effector. In addition, the number of switchings is reduced (9 times less) compared to PWM and ST approaches thus yielding a quieter behavior (see N_s in Table 3). The on-off control signals of the four cold-gas thrusters are depicted in Fig. 5 for the three strategies.

5. CONCLUSION

In this paper, two approaches are compared in order to damp the vibrations of a elastic CDPR using on-off actuators: a two-stage control strategy (with PWM and Schmitt trigger modulation) and a MIQP-based MPCA strategy. Both methods are validated in simulation. The proposed predictive strategy handles explicitly the actuator binary constraints and clearly yields better results on different aspects: faster rejection, least number of switchings of the binary actuators, reduced energy consumption and smallest position error.

Experimental results have been conducted for the first approach in Sellet et al. (2019). The predictive approach has not been evaluated experimentally for now, but is planned as future work. We are working on the real-time implementation of the MIQP problem, since the current implementation used in the simulation is not real-time

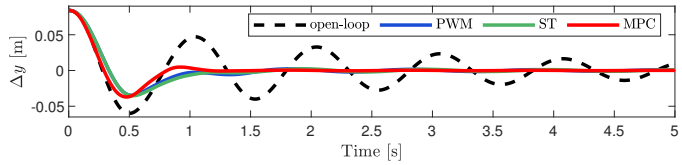

(a) Translational deviation Δy

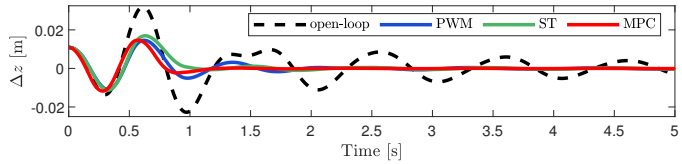

(b) Translational deviation Δz

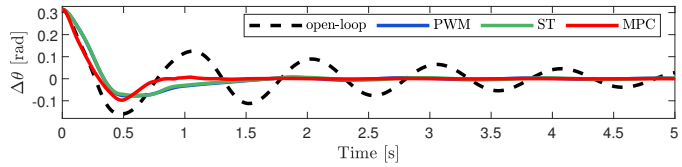

(c) Angular position deviation $\Delta\theta$

Fig. 4. Simulation results: measurement signals.

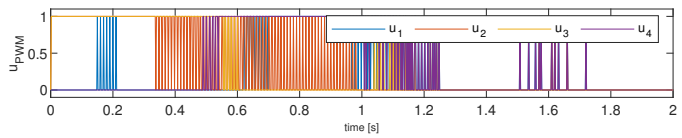

(a) UFGs Inputs PWM

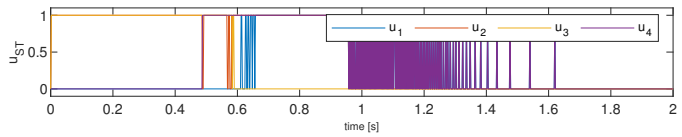

(b) UFGs Inputs ST

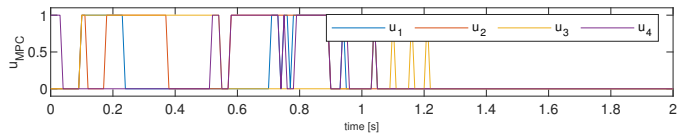

(c) UFGs Inputs MPC

Fig. 5. Simulation results: control signals.

compatible. We are also evaluating the ACADO toolkit (Quirynen et al. (2015)) that generates C code of fast solvers for nonlinear MPC problem with constraints.

REFERENCES

Allan, D.A., Risbeck, M.J., and Rawlings, J.B. (2016). Stability and robustness of model predictive control with discrete actuators. In *2016 American Control Conference (ACC)*, 32–37. IEEE.

Bächle, T., Graichen, K., Buchholz, M., and Dietmayer, K. (2015). Model predictive control allocation in electric vehicle drive trains. *IFAC-PapersOnLine*, 48(15), 335–340.

Begey, J., Cuvillon, L., Lesellier, M., Gouttefarde, M., and Gangloff, J. (2018). Dynamic control of parallel robots driven by flexible cables and actuated by position-controlled winches. *IEEE Transactions on Robotics*, 35(1), 286–293.

Behzadipour, S. and Khajepour, A. (2006). Stiffness of cable-based parallel manipulators with application to stability analysis. *Journal of mechanical design*, 128(1), 303–310.

Bemporad, A. and Morari, M. (1999). Control of systems integrating logic, dynamics, and constraints. *Automatica*, 35(3), 407–427.

Bemporad, A. and Naik, V.V. (2018). A numerically robust mixed-integer quadratic programming solver for embedded hybrid model predictive control. *IFAC-PapersOnLine*, 51(20), 412–417.

Gangloff, J. (2016). Raspberry Pi Simulink coder target (RPIt). `https://github.com/jacqu/rpit`.

Johansen, T.A. and Fossen, T.I. (2013). Control allocationa survey. *Automatica*, 49(5), 1087–1103.

Lesellier, M., Cuvillon, L., Gangloff, J., and Gouttefarde, M. (2018). An active stabilizer for cable-driven parallel robot vibration damping. In *2018 IEEE/RSJ International Conference on Intelligent Robots and Systems (IROS)*, 5063–5070. IEEE.

Löfberg, J. (2004). YALMIP : A toolbox for modeling and optimization in MATLAB. In *In Proceedings of the CACSD Conference*. Taipei, Taiwan.

Luo, Y., Serrani, A., Yurkovich, S., Doman, D.B., and Oppenheimer, M.W. (2004). Model predictive dynamic control allocation with actuator dynamics. In *Proceedings of the 2004 American control conference*, volume 2, 1695–1700. IEEE.

Maciejowski, J.M. (2002). *Predictive control: with constraints*. Pearson education.

Qi, R., Rushton, M., Khajepour, A., and Melek, W.W. (2019). Decoupled modeling and model predictive control of a hybrid cable-driven robot. *Robotics and Autonomous Systems*, 118, 1–12.

Qian, S., Zi, B., Shang, W.W., and Xu, Q.S. (2018). A review on cable-driven parallel robots. *Chinese Journal of Mechanical Engineering*, 31(1), 66.

Qian, X., Altché, F., Bender, P., Stiller, C., and de La Fortelle, A. (2016). Optimal trajectory planning for autonomous driving integrating logical constraints: An MIQP perspective. In *2016 IEEE 19th International Conference on Intelligent Transportation Systems (ITSC)*, 205–210. IEEE.

Quirynen, R., Vukov, M., Zanon, M., and Diehl, M. (2015). Autogenerating microsecond solvers for nonlinear mpc: a tutorial using acado integrators. *Optimal Control Applications and Methods*, 36(5), 685–704.

Sellet, H., Khayour, I., Cuvillon, L., Durand, S., and Gangloff, J. (2019). Active damping of parallel robots driven by flexible cables using cold-gas thrusters. In *2019 International Conference on Robotics and Automation (ICRA)*, 530–536. IEEE.

Siciliano, B. and Khatib, O. (2008). *Springer Handbook of Robotics*. Springer.

Veksler, A., Johansen, T.A., Borrelli, F., and Realfsen, B. (2016). Dynamic positioning with model predictive control. *IEEE Transactions on Control Systems Technology*, 24(4), 1340–1353.

Weber, X., Cuvillon, L., and Gangloff, J. (2014). Active vibration canceling of a cable-driven parallel robot using reaction wheels. In *Proc. IEEE/RSJ Int. Conf. Intelligent Robots and Systems*, 1724–1729. doi: 10.1109/IROS.2014.6942787.